

Critical excitation-rate enhancement of a dipolar scatterer close to a plasmonic nanosphere and importance of multipolar self-coupling

Faezeh Tork Ladani, Salvatore Campione,^{*} Caner Guclu,[†] and Filippo Capolino[‡]*Department of Electrical Engineering and Computer Science, University of California Irvine, Irvine, California 92697 USA*

(Received 18 October 2013; revised manuscript received 30 July 2014; published 16 September 2014)

We develop an electrodynamic model based on dyadic Green's functions for analyzing the near-field interactions between a dipolar scatterer (DS) and a plasmonic nanosphere (PN) under external excitation, accounting for multipolar contributions in the evaluation of the scattered fields. In particular, we include all the radiative and nonradiative field interactions between the DS and the PN, particularly the physical mechanism of DS's self-coupling through the PN, which is either neglected or approximated in previous work. Our objective is to show under which conditions self-coupling is important for strong excitation-rate enhancement of the DS and provide a description of the system's properties. We analytically investigate the conditions under which the excitation rate of a DS, such as an organic dye or a quantum dot, is enhanced when located in close proximity to a PN. We show the existence of *critical conditions* in terms of polarizabilities and distances that lead to large enhancement based on self-coupling and how to predict it.

DOI: [10.1103/PhysRevB.90.125127](https://doi.org/10.1103/PhysRevB.90.125127)

PACS number(s): 73.20.Mf, 78.67.Bf

I. INTRODUCTION

Nanoscatterers such as molecular dyes and quantum dots (QDs) have recently been of great interest in view of their ample range of applicability, including spectroscopy, imaging, single-molecule resolution, quantum cryptography, metrology, and solar cells [1–4]. Such nanoscatterers are, in general, well described by dipolar-like scattering processes at optical frequencies. Accordingly, using a single-dipole approximation (SDA) [5,6], the induced electric dipole moment of such (molecular dye or QD) scatterers is given by $\mathbf{p} = \underline{\alpha}_{\text{DS}} \cdot \mathbf{E}_{\text{loc}}$, where \mathbf{E}_{loc} is the local electric field at the dipole scatterer (DS) location, and $\underline{\alpha}_{\text{DS}}$ is its electric polarizability tensor. From this description one may infer that the strength of the dipolar response ultimately depends on both the electric polarizability $\underline{\alpha}_{\text{DS}}$ and the strength of the local electric field \mathbf{E}_{loc} acting on the DS. Since these DSs generally have a small polarizability associated with their small size, one needs to largely increase the local electric field, \mathbf{E}_{loc} , in order to induce significant dipole moment strength.

One way to greatly increase the local electric field involves the use of plasmonic nanospheres (PNs) close to their resonance frequency (whose value is dictated by shape, material, and size). Systems comprising PNs and DSs have been under fervent studies in recent years. Beside the advantage in terms of field-enhancement applications, PNs-DSs combinations have been suggested also for loss compensation in metamaterials [7–11], because losses would otherwise hinder several of the promising features of metamaterials, such as subwavelength resolution and cloaking. This fact puts in evidence the importance of studying the interaction between DSs and PNs. Many articles have been devoted to the investigation of radiative and nonradiative decay rates and to the

emission enhancement of molecules beside metallic nanoparticles numerically, theoretically, or experimentally [12–21]. Also, studies have reported on the near-field effect of molecules on metallic structures [22–24].

These contributions notwithstanding, we believe that currently there is a need to better understand the near-field interactions between a DS and a PN to compute the DS's excitation rate, introduced in the next section. From a physical point of view, the coupling between DS and PN through the scattering process introduces a *feedback loop* (consisting of the back-and-forth scattering between DS and PN) that can *build up* a strong field at the DS location under proper or *critical* conditions, as we will call them in later sections. This feedback mechanism, which we refer to as the *self-coupling* of the DS, is summarized as follows: the DS scatters waves toward the PN that are rescattered by the PN local plasmon, building up even a stronger field at the DS location as a result of constructive superposition. In classical terms, the intensity of the electric field increases in this scenario. Critical conditions are defined such that this feedback mechanism is strong enough to lead to strong local fields at the DS location. In the feedback mechanism, the DS polarizability plays a key role together with the distance between DS and PN. That is why we introduce the concepts of critical distance and critical polarizability. We rely on an analytical method based on Green's functions (GFs) to perform an accurate analysis of this setup. In particular, we account for the multipolar effects in the GF representing the scattering from the PN for calculating the DS self-coupling. In other words, the contribution of the DS's scattering to its own local field, through the interaction with the PN, is here represented using GF theory. To the authors' knowledge, this has been neglected in most of the previous work dealing with systems as described in this paper, or accounted for by using some approximations. For example, in Ref. [17] the authors investigated Raman scattering of molecules located very close to a nanosphere, and since the latter is much larger than a molecule, it was locally approximated as a planar surface for self-coupling calculations. As we show in this paper, a more accurate analysis is necessary to observe further enhancement of the local electric field due to self-coupling

^{*}Current address: Center for Integrated Nanotechnologies (CINT), Sandia National Laboratories, P.O. Box 5800, Albuquerque, NM, 87185, USA.

[†]cgclu@uci.edu

[‡]f.capolino@uci.edu

(which boosts the DS's excitation rate) that cannot be observed under the planar approximation mentioned above. In particular, we show in this paper the existence of *critical conditions* in terms of polarizabilities and distances that lead to large DS's excitation-rate enhancement, based on self-coupling taking into account multipolar contributions. It follows that in certain cases neglecting the self-coupling may lead to inaccurate results, and thus cannot predict the critical enhancements. We will also briefly show that Rabi-like splitting [25–29] may appear close to the critical conditions when looking at the frequency response of the system.

As a strong motivation and rationale for our analysis, the development of smaller PNs, the ability to place DSs at nanometer distances from PNs, and stronger DSs (e.g., quantum dots) devised in recent articles [30,31] suggests that both scattering processes associated to DS and PN will become comparable, and all the interactions should be included for accurate estimations.

The structure of the paper is as follows. We introduce in Sec. II the formalism used for modeling the local-field enhancement for a system comprising a PN-DS pair under plane-wave incidence. In Sec. III, we investigate the special case where the incident electric field is polarized along the axis on which DS and PN lay. Having introduced the concepts of critical polarizability and critical distance in Sec. III, in Sec. IV we then discuss practical DSs (a Rhodamine 6G dye molecule and a CdSe QD) and observe the effect of self-coupling on their excitation-rate enhancements, emphasizing the importance of multipolar contributions in field evaluation. Finally, in Sec. V we discuss the physical conditions (in terms of DS polarizability and geometrical parameters) required to achieve strong critical enhancements through self-coupling. Final remarks are then provided in Sec. VI.

II. EXCITATION-RATE ENHANCEMENT AND THEORETICAL MODEL EMPLOYING DYADIC GREEN'S FUNCTIONS

It is our aim to understand how the self-coupling mechanism impacts the DS's excitation rate. The excitation rate γ_{exc} of a DS, like an organic dye or a QD, is proportional to the power absorbed by the DS itself as $\gamma_{\text{exc}} \propto |\hat{\mathbf{n}}_p \cdot \mathbf{E}_{\text{loc}}|^2$ [1], where the unit vector $\hat{\mathbf{n}}_p$ represents the dipolar direction of the DS and \mathbf{E}_{loc} is the local field acting on it. This formula shows that γ_{exc} is proportional to the intensity of the component of the local electric field at the DS location aligned with the DS absorption dipole moment [14,32–34]. Furthermore, the enhancement of the excitation rate γ_{exc}^n is defined as

$$\gamma_{\text{exc}}^n = \frac{\gamma_{\text{exc}}}{\gamma_{\text{exc}}^0} = \frac{|\hat{\mathbf{n}}_p \cdot \mathbf{E}_{\text{loc}}(\mathbf{r})|^2}{|\hat{\mathbf{n}}_p \cdot \mathbf{E}_{\text{inc}}(\mathbf{r})|^2}, \quad (1)$$

where $\gamma_{\text{exc}}^0 \propto |\hat{\mathbf{n}}_p \cdot \mathbf{E}_{\text{inc}}|^2$ is the excitation rate of the DS in free space (i.e., in absence of the PN), when the DS is excited by the incident field \mathbf{E}_{inc} . Therefore, to estimate the enhancement, γ_{exc}^n , which is the fundamental parameter studied in this paper, we need to evaluate the local electric field $\mathbf{E}_{\text{loc}}(\mathbf{r})$ at the DS location in presence of the PN.

Consider the setup in Fig. 1, where a DS is located at position \mathbf{r} in proximity of a PN centered at the origin $\mathbf{0}$ of the

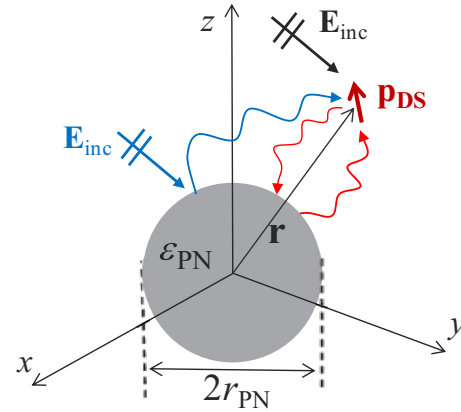


FIG. 1. (Color online) An arbitrarily polarized dipolar scatterer (DS, with the induced dipole moment \mathbf{p}_{DS}) beside a plasmonic nanosphere (PN) under plane wave incidence. Different scattering mechanisms contributing to the local electric field at the DS location are illustrated.

chosen reference system. The local field

$$\mathbf{E}_{\text{loc}}(\mathbf{r}) = \mathbf{E}_{\text{inc}}(\mathbf{r}) + \underline{\mathbf{G}}_0(\mathbf{r}, \mathbf{0}) \cdot \mathbf{p}_{\text{PN}} + \underline{\mathbf{G}}_{\text{sc}}(\mathbf{r}, \mathbf{r}) \cdot \mathbf{p}_{\text{DS}} \quad (2)$$

at the DS location is given by three contributions, namely (i) the incident plane wave $\mathbf{E}_{\text{inc}}(\mathbf{r})$ acting directly on the DS (depicted in black in Fig. 1); (ii) the field scattered by the PN upon plane-wave incidence (depicted in blue in Fig. 1), and (iii) the scattering of the PN when illuminated by the near field of the DS, i.e., the self-coupling (depicted in red in Fig. 1).

To evaluate the second contribution in Eq. (2), induced by the incident plane wave, we model the PN located at the origin as an electric dipole with dipole moment $\mathbf{p}_{\text{PN}} = \alpha_{\text{PN}} \mathbf{E}_{\text{inc}}(\mathbf{0})$, where α_{PN} is the PN dipolar Mie polarizability [5,7]. The PN scattered field evaluated at the DS location \mathbf{r} is calculated as $\underline{\mathbf{G}}_0(\mathbf{r}, \mathbf{0}) \cdot \mathbf{p}_{\text{PN}}$, where $\underline{\mathbf{G}}_0(\mathbf{r}, \mathbf{0})$ is the free-space dyadic GF (see the Appendix for more details). The PN dipolar model is sufficiently accurate as long as the PN is of subwavelength dimensions, as in our case. The third contribution in Eq. (2) is due to the self-coupling and is evaluated as $\underline{\mathbf{G}}_{\text{sc}}(\mathbf{r}, \mathbf{r}) \cdot \mathbf{p}_{\text{DS}}$, where $\mathbf{p}_{\text{DS}} = \underline{\alpha}_{\text{DS}} \cdot \mathbf{E}_{\text{loc}}(\mathbf{r})$ is the DS electric dipole at \mathbf{r} and $\underline{\alpha}_{\text{DS}}$ is the DS polarizability tensor, and $\underline{\mathbf{G}}_{\text{sc}}(\mathbf{r}, \mathbf{r})$ is the PN-scattering dyadic GF [35] (see the Appendix for more details), used for evaluating the scattered electric field at \mathbf{r} produced by a dipole at the same location. The evaluation of the self-coupling term demands the evaluation of the scattering GF, $\underline{\mathbf{G}}_{\text{sc}}(\mathbf{r}, \mathbf{r})$, now assuming both source and observation in the very near zone of the PN, hence it needs to account for several multipolar terms. These multipolar terms are responsible for radiative and nonradiative (i.e., evanescent) coupling to the DS. In the simulations that follow, we will denote with N the number of multipolar terms chosen to guarantee convergence of the GF summations (see Sec. IV B for more details).

By combining Eq. (2) with $\mathbf{p}_{\text{PN}} = \alpha_{\text{PN}} \mathbf{E}_{\text{inc}}(\mathbf{0})$ and $\mathbf{p}_{\text{DS}} = \underline{\alpha}_{\text{DS}} \cdot \mathbf{E}_{\text{loc}}(\mathbf{r})$, one obtains the closed-form expression for the local field

$$\mathbf{E}_{\text{loc}}(\mathbf{r}) = [\mathbf{I} - \underline{\mathbf{G}}_{\text{sc}}(\mathbf{r}, \mathbf{r}) \cdot \underline{\alpha}_{\text{DS}}]^{-1} \mathbf{E}_1(\mathbf{r}) \quad (3)$$

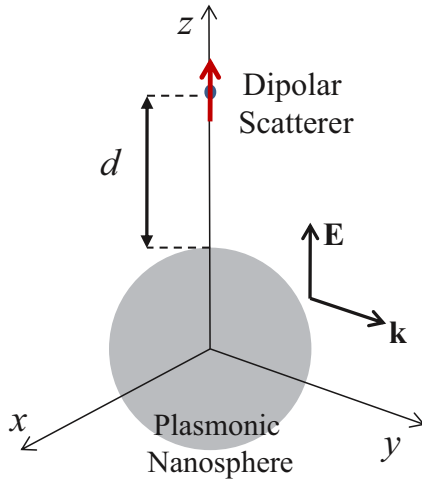


FIG. 2. (Color online) Setup under analysis: A z -polarized DS beside PN illuminated by a plane wave traveling along y with electric field polarized along z . The DS is at a distance d from the PN surface.

where, importantly,

$$\mathbf{E}_1(\mathbf{r}) = \mathbf{G}_0(\mathbf{r}, \mathbf{0}) \cdot \mathbf{p}_{\text{PN}} + \mathbf{E}_{\text{inc}}(\mathbf{r}) \quad (4)$$

is the local field at the DS location that one would have if self-coupling were neglected. Therefore, the term $[\mathbf{I} - \mathbf{G}_{\text{sc}}(\mathbf{r}, \mathbf{r}) \cdot \underline{\alpha}_{\text{DS}}]^{-1}$ in Eq. (3) represents the factor due to self-coupling. In general, if the product $\mathbf{G}_{\text{sc}}(\mathbf{r}, \mathbf{r}) \cdot \underline{\alpha}_{\text{DS}}$ is negligible, it follows that $[\mathbf{I} - \mathbf{G}_{\text{sc}}(\mathbf{r}, \mathbf{r}) \cdot \underline{\alpha}_{\text{DS}}]^{-1} \approx \mathbf{I}$ and $\mathbf{E}_{\text{loc}}(\mathbf{r}) \approx \mathbf{E}_1(\mathbf{r})$ as assumed in previous work, for instance in Ref. [14].

For simplicity, consider the setup in Fig. 2, where we assume the DS located along the z axis at a distance d from the surface of the PN, and we assume that the DS has dipole moment along the r direction as the polarizability is $\underline{\alpha}_{\text{DS}} = \alpha_{\text{DS}} \hat{\mathbf{r}}$. Assuming an $\exp(-i\omega t)$ time harmonic convention, the DS-PN system is illuminated by a z -polarized plane wave $\mathbf{E}_{\text{inc}}(\mathbf{r}) = E_0 \hat{\mathbf{z}} e^{iky}$ traveling along the y direction with wavenumber $k = \omega \sqrt{\epsilon_0 \epsilon_h \mu_0}$, where ϵ_h is the host relative permittivity, and E_0 is the plane-wave amplitude, with electric field polarized along the r direction at the location of the DS. This is a configuration that leads to large excitation-rate enhancement γ_{exc}^n [14,16]. Under these assumptions, and considering that in this case $\hat{\mathbf{n}}_p = \hat{\mathbf{r}}$, the excitation-rate enhancement γ_{exc}^n in Eq. (1) takes the form

$$\gamma_{\text{exc}}^n = \left| \frac{1 + \alpha_{\text{PN}} G_0^{rr}(\mathbf{r}, \mathbf{0})}{1 - \alpha_{\text{DS}} G_{\text{sc}}^{rr}(\mathbf{r}, \mathbf{r})} \right|^2, \quad (5)$$

where the superscript rr refers to the $\hat{\mathbf{r}}\hat{\mathbf{r}}$ entry of the dyadic GFs (as shown in the Appendix, a spherical representation of the dyadic GF is convenient). We then express the excitation-rate enhancement as

$$\gamma_{\text{exc}}^n = \chi \bar{\gamma}_{\text{exc}}^n, \quad (6)$$

where

$$\bar{\gamma}_{\text{exc}}^n = \left| \frac{\hat{\mathbf{n}}_p \cdot \mathbf{E}_1(\mathbf{r})}{\hat{\mathbf{n}}_p \cdot \mathbf{E}_{\text{inc}}(\mathbf{r})} \right|^2 = |1 + \alpha_{\text{PN}} G_0^{rr}(\mathbf{r}, \mathbf{0})|^2 \quad (7)$$

is the excitation-rate enhancement neglecting self-coupling and

$$\chi = \frac{1}{|1 - \alpha_{\text{DS}} G_{\text{sc}}^{rr}(\mathbf{r}, \mathbf{r})|^2} \quad (8)$$

denotes the factor due to the self-coupling, which may lead to even further enhancement. Note that if we assume that self-coupling is negligible, one has $\chi \approx 1$, which implies that $\mathbf{E}_{\text{loc}}(\mathbf{r}) \approx \mathbf{E}_1(\mathbf{r})$, and the excitation-rate enhancement is approximated by $\gamma_{\text{exc}}^n \approx \bar{\gamma}_{\text{exc}}^n$, which coincides with what is reported in [1,14].

As it will be shown next, there are conditions (here called critical conditions) that lead to strong enhancement exploiting the self-coupling factor. Beside the DS polarizability, different parameters of the plasmonic scatterer, such as material, shape, and size, and also the distance between the DS and the scatterer play a role via $G_{\text{sc}}^{rr}(\mathbf{r}, \mathbf{r})$ in maximizing χ . In other words, through $G_{\text{sc}}^{rr}(\mathbf{r}, \mathbf{r})$ we provide a mathematical representation of the feedback mechanism between DS and PN. In this paper, we fix the shape (sphere) and the material of the plasmonic nanoparticle (gold) and thus define the critical DS polarizability and distance that lead to critical enhancement of the excitation rate. The formalism adopted here can be also applied to other shapes of nanoantennas, such as the bowtie nanoantenna [36,37]. In these more general cases the GF can be found numerically, via full-wave simulations, and the same concepts developed here can be applied to maximize the enhancement.

In all the results presented in the following sections we assume the PN is made of gold with complex values of permittivity taken from experimental data tabulated in Ref. [38].

III. CRITICAL POLARIZABILITY AND CRITICAL DISTANCE

A. Dependence on geometrical parameters at a constant frequency

We consider here the complex DS polarizability $\alpha_{\text{DS}} = \alpha'_{\text{DS}} + i\alpha''_{\text{DS}}$, assuming $\alpha''_{\text{DS}}/\alpha'_{\text{DS}} = 10^{-2}$, at 568 THz (free space wavelength of 528 nm), and $d = 2$ nm. The wavelength of 528 nm is close to the PN resonance wavelength, the latter rather insensitive to the particle size itself, as, for example, described in Ref. [39]. We include $N = 60$ PN multipoles in the calculation of $G_{\text{sc}}^{rr}(\mathbf{r}, \mathbf{r})$ to guarantee convergence (see Sec. IV B for more details). We thus report in Fig. 3(a) the excitation-rate enhancement γ_{exc}^n in logarithmic scale versus the PN radius r_{PN} and the magnitude of the DS polarizability $|\alpha_{\text{DS}}|$ (the distance d is kept constant). First, one should note that thanks to the PN, excitation-rate enhancements of 10–30 folds are easily obtained. One should also note that γ_{exc}^n is largely enhanced (up to 1000 folds) for a certain range of critical polarizabilities close to $|\alpha_{\text{DS}}| \approx 8.5 \times 10^{-36} [\text{Fm}^2]$, and that this is almost independent of the PN radius r_{PN} . At least 30 folds of this total enhancement is due to self-coupling, as verified by the graph in Fig. 3(b), where also χ in Eq. (8) is plotted versus r_{PN} and $|\alpha_{\text{DS}}|$. Therefore, we show that self-coupling cannot be neglected in the evaluation of γ_{exc}^n for a critical DS polarizability range. We also report in Fig. 3(c) a similar plot showing the term $\bar{\gamma}_{\text{exc}}^n$ in Eq. (7), which

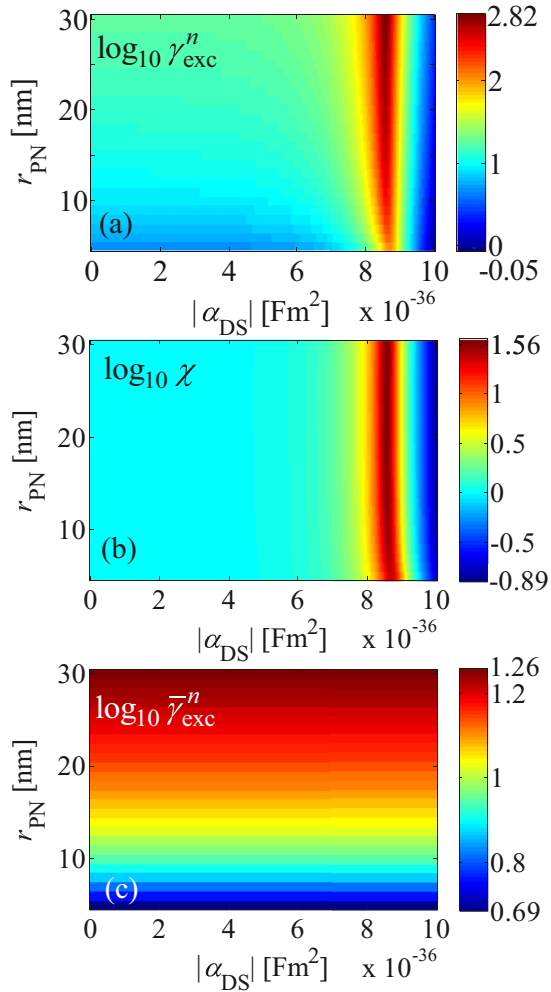


FIG. 3. (Color online) (a) Excitation-rate enhancement γ_{exc}^n (logarithmic scale) versus r_{PN} and $|\alpha_{\text{DS}}|$. As in (a), for (b) the self-coupling term χ in Eq. (8) and for (c) the term $\bar{\gamma}_{\text{exc}}^n$ in Eq. (7). Simulation parameters: $\varepsilon_h = 1$, $d = 2$ nm, and the frequency is 568 THz (528 nm). Note also the different scales in (a)–(c) for clarity of presentation of the results.

represents the excitation-rate enhancement when self-coupling is neglected, i.e., when assuming that $\mathbf{E}_{\text{loc}}(\mathbf{r}) \approx \mathbf{E}_1(\mathbf{r})$ in Eq. (3); the result shows that $\bar{\gamma}_{\text{exc}}^n$ cannot recover γ_{exc}^n correctly in the critical DS polarizability range. Indeed, note how in Fig. 3(c) $\bar{\gamma}_{\text{exc}}^n$ increases for increasing radius r_{PN} , and it does not depend on the DS polarizability α_{DS} . The result in Fig. 3 makes us infer that, at a fixed distance, there exists a range of critical polarizabilities for which self-coupling is a major contribution in excitation-rate enhancement (especially for small radius r_{PN}) and here it can provide with an additional 30-fold enhancement. However, Fig. 3(b) also shows that self-coupling can be detrimental to the excitation rate when the DS polarizability assumes very large values, i.e., $\gamma_{\text{exc}}^n < \bar{\gamma}_{\text{exc}}^n$ because $\chi < 1$.

In practical scenarios, we deal with given DS properties, while the critical polarizability concept depends on the plasmonic system as a whole. Therefore, for any given DS, the system at hand (PN geometry, material, and distance d) should be designed such that the DS polarizability is within the range

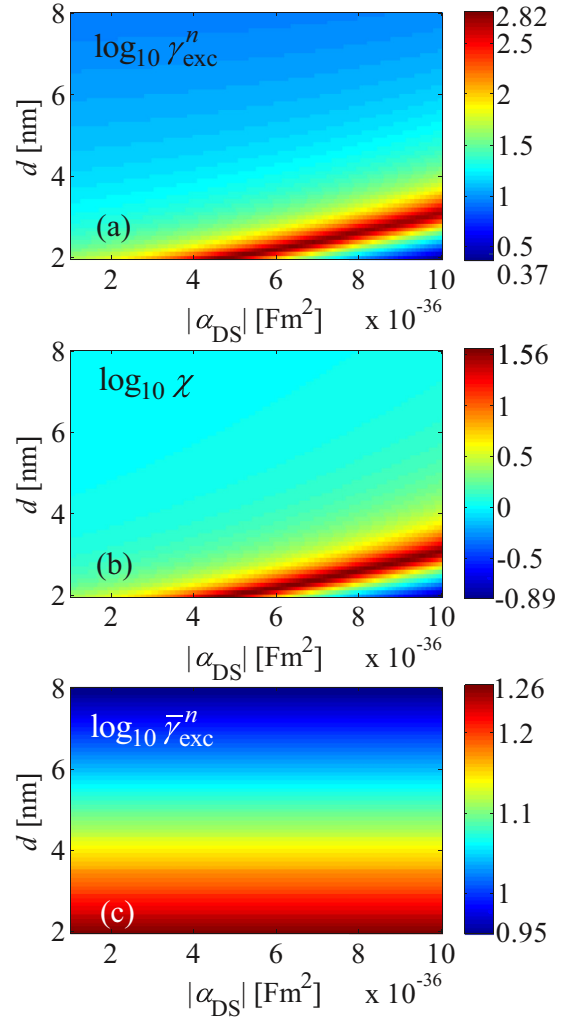


FIG. 4. (Color online) As described in the caption of Fig. 3, versus d and $|\alpha_{\text{DS}}|$. Simulation parameters: $r_{\text{PN}} = 30$ nm; all other parameters are as described in the caption of Fig. 3. Note also the different scales in (a)–(c) for clarity of presentation of the results.

of critical polarizabilities of the system. Next, considering the DS located at a distance $|\mathbf{r}| = r_{\text{PN}} + d$ from the origin on $+z$ axis, we investigate the excitation-rate enhancement dependence on the distance d and the DS polarizability, keeping r_{PN} fixed. Figure 4 shows the excitation-rate enhancement γ_{exc}^n , the self-coupling term χ , and $\bar{\gamma}_{\text{exc}}^n$ versus distance d and polarizability $|\alpha_{\text{DS}}|$, assuming a plasmonic nanosphere with $r_{\text{PN}} = 30$ nm (all other parameters are as in Fig. 3). We note now the presence of interrelated critical distance and critical polarizability for which γ_{exc}^n assumes the largest values. A considerable amount of this enhancement is again attributed to the self-coupling term χ as observed in Fig. 4(b). Note also that when the DS is far from the PN, with larger and larger d , the contribution of self-coupling χ to γ_{exc}^n becomes negligible. Figure 4(c) shows that, when neglecting the self-coupling term, the excitation-rate enhancement $\bar{\gamma}_{\text{exc}}^n$ increases as long as the DS gets closer to the PN, in agreement with the observations in Refs. [14,16,40]. Instead, when considering self-coupling whose impact is reported in Fig. 4(b), χ is responsible of even 30 folds of enhancement at the maximum obtained in

correspondence of a critical distance. However, self-coupling can also be detrimental to the excitation rate. Indeed, when assuming large DS polarizability values, Fig. 4(b) also shows that very short distances lead to less enhancement (i.e., $\gamma_{\text{exc}}^n < \bar{\gamma}_{\text{exc}}^n$) because there $\chi < 1$.

We want to emphasize that the values of critical polarizability, though large in general, are still rather small when compared to the PN polarizability as $|\alpha_{\text{DS}}/\alpha_{\text{PN}}| \approx 10^{-3}$; for such values, we have found the critical distance to be about 2 to 3 nm, which is a promising result paving the way for realizable applications employing fluorescent molecules or QDs.

B. Dependence on DS polarizability frequency dispersion

We consider here the DS polarizability having a Lorentzian frequency dependence given by

$$\alpha_{\text{DS}} = \alpha'_{\text{DS}} + i\alpha''_{\text{DS}} = \frac{\alpha_0 \omega_0^2}{\omega_0^2 - \omega^2 - i\gamma\omega} + \alpha_\infty, \quad (9)$$

where ω_0 is the transition angular frequency, γ is the linewidth (or damping factor), α_∞ is the high frequency limit of the polarizability, and $\alpha_0 + \alpha_\infty$ is the static polarizability.

The parameters used for DS polarizability here are chosen as $\alpha_0 = 7.31 \times 10^{-38}$ [Fm²], $\alpha_\infty = 5.37 \times 10^{-36}$ [Fm²], $\omega_0 = 2\pi(616) \times 10^{12}$ [rad/s], and $\gamma = 12.14 \times 10^{13}$ [rad/s], leading to the real and imaginary parts of the DS polarizability reported in Fig. 5. The parameters of the DS polarizability reported above are chosen to match the polarizability of a realistic QD around its resonance frequency at 616 THz [8]. The real part $\alpha'_{\text{DS}} \approx 5 \times 10^{-36}$ [Fm²] is rather constant with frequency but in the vicinity of the Lorentzian transition angular frequency ω_0 (where, however, its value does not vary much) and it is close in value to the critical polarizability introduced in Sec. III A (Fig. 3), thus we expect to find large enhancements for d close to 2 nm. On the other hand, the imaginary part α''_{DS} peaks at 616 THz exhibiting values in the same order of α'_{DS} around the resonance, otherwise being negligible. Note also that considering a gold PN with radius $r_{\text{PN}} = 30$ nm the PN Mie polarizability has a resonance peak at 579 THz with $|\alpha_{\text{PN}}| = 5.76 \times 10^{-33}$ [Fm²].

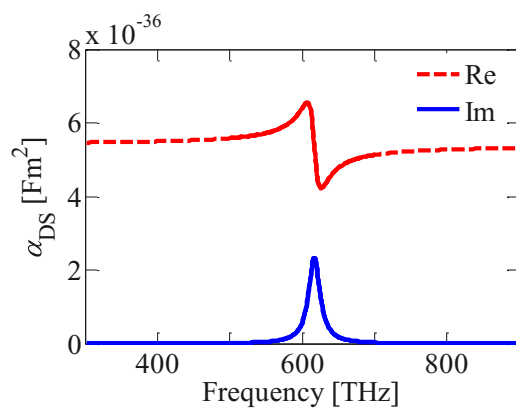


FIG. 5. (Color online) Real and imaginary parts of α_{DS} versus frequency assuming a Lorentzian shape as in Eq. (9) with the parameters given in the text.

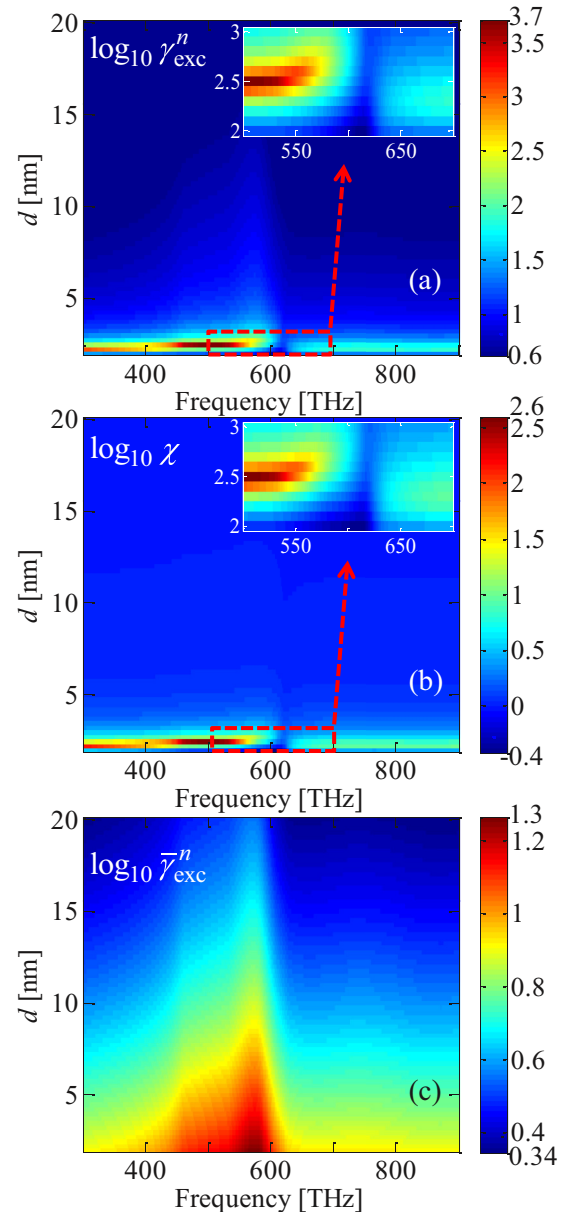


FIG. 6. (Color online) (a) Excitation-rate enhancement γ_{exc}^n (logarithmic scale) versus d and frequency. (b) As in (a), for the term χ in Eq. (8) and (c) for $\bar{\gamma}_{\text{exc}}^n$ in Eq. (7). Note also the different scales in (a)–(c) for clarity of presentation of the results.

Under these conditions, we show in Fig. 6 the excitation-rate enhancement γ_{exc}^n in Eq. (6), χ in Eq. (8), and $\bar{\gamma}_{\text{exc}}^n$ in Eq. (7) versus d and frequency. It can be seen that for DS in close proximity of the PN (d about 2.5 nm), self-coupling has the dominant effect, yielding $\gamma_{\text{exc}}^n \approx 5000$ in contrast to $\bar{\gamma}_{\text{exc}}^n \approx 12$, showing that almost a 400-fold increase is due to self-coupling χ , hence indicating its importance in understanding the electrodynamic interactions of a PN-DS system. However, the impact of self-coupling decreases dramatically when the imaginary part of α_{DS} peaks around 616 THz, as shown by the dark blue area in Figs. 6(a) and 6(b) insets. This resonance splitting in the spectrum is a signature of Rabi-like splitting, indicating strong coupling regime between the DS and the PN.

Further discussion on optimal values is provided in Sec. V. Looking at Fig. 6(c) one can also infer that when self-coupling is neglected, the excitation-rate enhancement $\bar{\gamma}_{\text{exc}}^n$ is only due to the plasmonic resonance of the PN, which occurs at 579 THz. In summary, the spectral description of a dye excitation rate can be wrongly estimated when neglecting the self-coupling physical mechanism, as one infers by comparing the values and the frequency descriptions in Figs. 6(a) and 6(b).

IV. DYE MOLECULE AND QUANTUM DOT AS DIPOLAR SCATTERERS

A. Examples of DS polarizabilities

Having established that both distance and DS polarizability dramatically affect the excitation-rate enhancement γ_{exc}^n , we turn our analysis to two cases of DS, namely we consider a fluorescent dye molecule Rhodamine 6G (R6G) and a CdSe QD in order to assess the necessity of the self-coupling term for practical systems. The polarizability of the R6G is evaluated via a Lorentzian oscillator model given in Eq. (9) [41,42], with the following parameters based on the data from Ref. [42] pp. 525–526 as, $\alpha_0 = 3.9 \times 10^{-39}$ [Fm²], $\alpha_\infty = 2.2 \times 10^{-39}$ [Fm²], $\omega_0 = 2\pi(569.94) \times 10^{12}$ [rad/s], and $\gamma = 235.4 \times 10^{12}$ [rad/s]. R6G dye polarizability has the value $\alpha_{\text{DS}} = (0.89 + i5.87) \times 10^{-38}$ [Fm²] at 568 THz (528 nm), corresponding to an absorption cross section of 0.08 nm². The polarizability of the chosen CdSe QD is instead modeled via Mie theory assuming a given permittivity, as done in Refs. [8,43–45], and has the value $\alpha_{\text{DS}} = (5.8 + i0.087) \times 10^{-36}$ [Fm²] associated to 0.1 nm² absorption cross section at 568 THz (528 nm). We have chosen this frequency of operation because it is close to the PN plasmonic resonance and because the higher imaginary part of the polarizability at higher frequency, e.g., 616 THz, may cause a sudden drop in excitation-rate enhancement as shown in Fig. 6(a).

We then show in Fig. 7 the excitation-rate enhancement γ_{exc}^n versus d for both R6G and CdSe QD for three cases: (i) we consider $N = 60$ multipolar terms in the computation of G_{sc}^{rr} (solid blue curve), leading to a relative error on $|G_{\text{sc}}^{rr}|$ less than 1.5%; (ii) we consider only the dipolar term (i.e., $N = 1$) in

G_{sc}^{rr} (dashed red curve); (iii) we neglect the self-coupling term [dotted green curve, that therefore represents $\bar{\gamma}_{\text{exc}}^n$ in Eq. (7)]. Since we considered a QD with a radius of 4 nm, the plot in Fig. 7(b) starts at $d = 4$ nm, i.e., the closest allowable distance of QD to the PN due to physical constraints. Similarly, in Fig. 7(a), the x axis starts at $d = 2$ nm, assuming that from such distance R6G dyes close to nanospheres can be still modeled as point dipoles as in Sec. II. We note that although in the case of R6G dye, the self-coupling term is negligible and does not contribute to γ_{exc}^n , in the QD case for very small distances we observe a value of about twice with respect to the case where self-coupling is neglected. We also note that the account of multipolar terms in the evaluation of G_{sc}^{rr} is found to be of vital importance, because such enhancement is not observed when only the dipolar term is accounted for ($N = 1$). This result shows that in certain practical cases self-coupling is important as it can induce a considerable variation in the excitation-rate enhancement γ_{exc}^n . Indeed, we infer from Figs. 3 and 4 that the value of the QD polarizability is within the range of critical polarizabilities, whereas the polarizability of R6G molecule is too small to generate enough scattering and hence $\chi \approx 1$. Since the QD's polarizability is larger than the R6G molecule's one, the QD sustains a stronger feedback mechanism with the PN than the R6G molecule does. The development of DS exhibiting critical polarizabilities with small volumes might open up to other scenarios where self-coupling is contributing, and even becomes the dominant process, for the excitation-rate enhancement γ_{exc}^n .

B. Importance of multipolar field contributions

As Fig. 7 shows, the self-coupling contribution manifests itself through multipolar scattering terms, whereas the dipolar term alone (i.e., $N = 1$) cannot represent the impact of self-coupling. We demonstrate the effect of the multipolar terms, providing a deeper insight into the physics of self-coupling in Fig. 8. The convergence of $G_{\text{sc}}^{rr}(\mathbf{r}, \mathbf{r})$, the $\hat{\mathbf{r}}\hat{\mathbf{r}}$ entry of the scattering dyadic GF, with respect to the number of considered multipoles plays a significant role. Recalling Eq. (8), we know that χ has an inverse dependence on $1 - \alpha_{\text{DS}} G_{\text{sc}}^{rr}(\mathbf{r}, \mathbf{r})$. Intuitively, one would correctly expect a large γ_{exc}^n when

$$\text{Re}\{\alpha_{\text{DS}} G_{\text{sc}}^{rr}(\mathbf{r}, \mathbf{r})\} \approx 1 \quad \text{and} \quad \text{Im}\{\alpha_{\text{DS}} G_{\text{sc}}^{rr}(\mathbf{r}, \mathbf{r})\} \ll 1 \quad (10)$$

Figures 8(a) and 8(b) show the real and imaginary parts of $\alpha_{\text{DS}} G_{\text{sc}}^{rr}(\mathbf{r}, \mathbf{r})$ versus number of multipoles N , for several radii of the PN. Distance is kept constant as $d = 2.5$ nm and $\alpha_{\text{DS}} = 6.8(1 + i0.01) \times 10^{-36}$ [Fm²] to be within the range of critical polarizabilities and distances as seen in Fig. 4(b). The first thing to be noted is that a larger number of multipoles is required for convergence when larger PNs are considered. For example, only about $N = 10$ multipoles are sufficient when $r_{\text{PN}} = 5$ nm, whereas about $N = 60$ multipoles are needed when $r_{\text{PN}} = 30$ nm. Remarkably, note how for the chosen distance (close in value to the critical distance for the adopted DS polarizability) $\text{Re}\{\alpha_{\text{DS}} G_{\text{sc}}^{rr}(\mathbf{r}, \mathbf{r})\} \approx 1$ and $\text{Im}\{\alpha_{\text{DS}} G_{\text{sc}}^{rr}(\mathbf{r}, \mathbf{r})\} \approx 0.2$, leading to the enhanced results in Fig. 4(b). [Note that the much smaller condition in Eq. (10) can be relaxed for achieving large enhancements, e.g., 30 folds, as it will be explained in Sec. V.] We want to stress that the achieved convergence of the scattering GF is a crucial concept

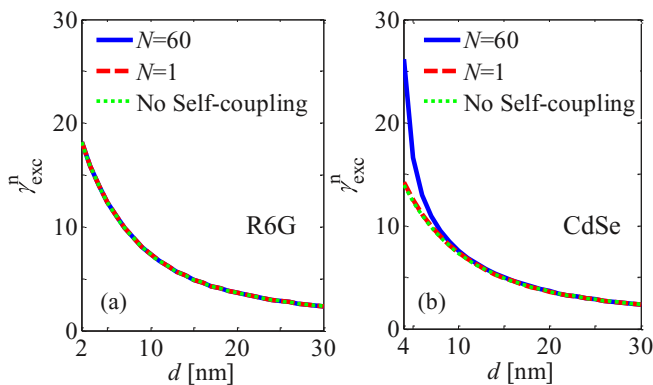


FIG. 7. (Color online) Excitation-rate enhancement γ_{exc}^n versus d for two realistic implementations of dipolar scatterers: (a) R6G and (b) CdSe QD. Simulation parameters: $\varepsilon_h = 1$, $r_{\text{PN}} = 30$ nm, and the frequency is 568 THz (528 nm). The variable N in the legend indicates the number of multipoles included in the calculation of G_{sc}^{rr} .

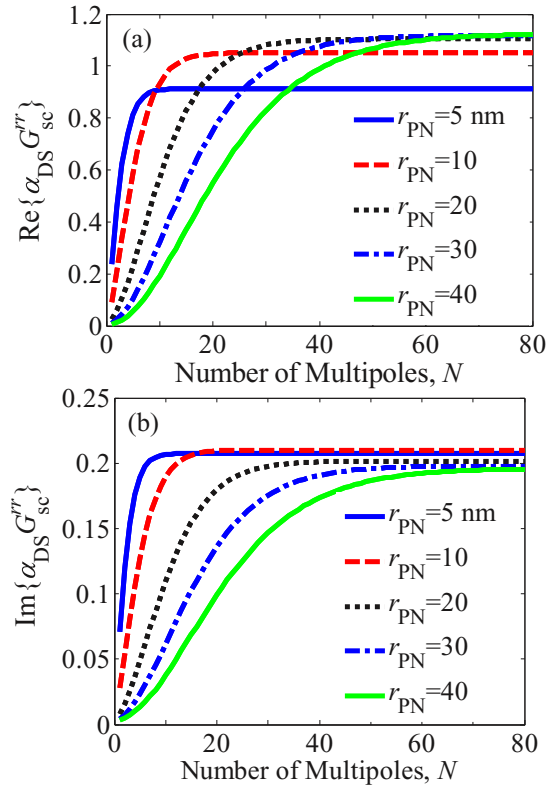


FIG. 8. (Color online) Convergence of G_{sc}^{rr} for $d = 2.5$ nm and various values of the PN radius r_{PN} .

in evaluating the self-coupling contribution: for example, in certain cases, a nonconverged summation may lead to the impression that the condition $\text{Re}\{\alpha_{DS} G_{sc}^{rr}(\mathbf{r}, \mathbf{r})\} = 1$ seems satisfied, leading to false estimation of large enhancement factors. For example, for the green curve in Fig. 8, relative to a PN with $r_{PN} = 40$ nm, calculations with only 40 multipoles seem to lead to such a critical condition, which is not correct since the converged value is achieved with about 70 multipoles.

As one would expect from previous analyses, convergence is also sensitive to d . We then plot in Figs. 9(a) and 9(b) the real and imaginary parts of $\alpha_{DS} G_{sc}^{rr}(\mathbf{r}, \mathbf{r})$ versus number of multipoles N , for several values of d . We clearly see that a slight variation in distance induces a major variation in the value assumed by $\text{Re}\{\alpha_{DS} G_{sc}^{rr}(\mathbf{r}, \mathbf{r})\}$ and $\text{Im}\{\alpha_{DS} G_{sc}^{rr}(\mathbf{r}, \mathbf{r})\}$, showing the criticality of d . Also note that more multipoles are needed as d decreases. We stress that $N = 60$ leads to an error on $|G_{sc}^{rr}|$ less than 1.5% for the smallest distance $d = 2$ nm analyzed in this paper.

V. DISCUSSION: IMPACT OF SCATTERING FOR SELF-COUPLING

We now turn our focus on the analysis of the complex-valued parameters in Eq. (5) to better understand critical polarizability and critical distance defined in Sec. III. We express the PN and DS polarizabilities as $\alpha_{PN} = \alpha'_{PN} + i\alpha''_{PN}$ and $\alpha_{DS} = \alpha'_{DS} + i\alpha''_{DS}$, where a prime and a double prime denote the real and the imaginary parts of the polarizabilities. Also, we separate the real and imaginary parts in the GFs as

$$G_{sc}^{rr}(\mathbf{r}, \mathbf{r}) = G'_{sc} + iG''_{sc} \quad (11)$$

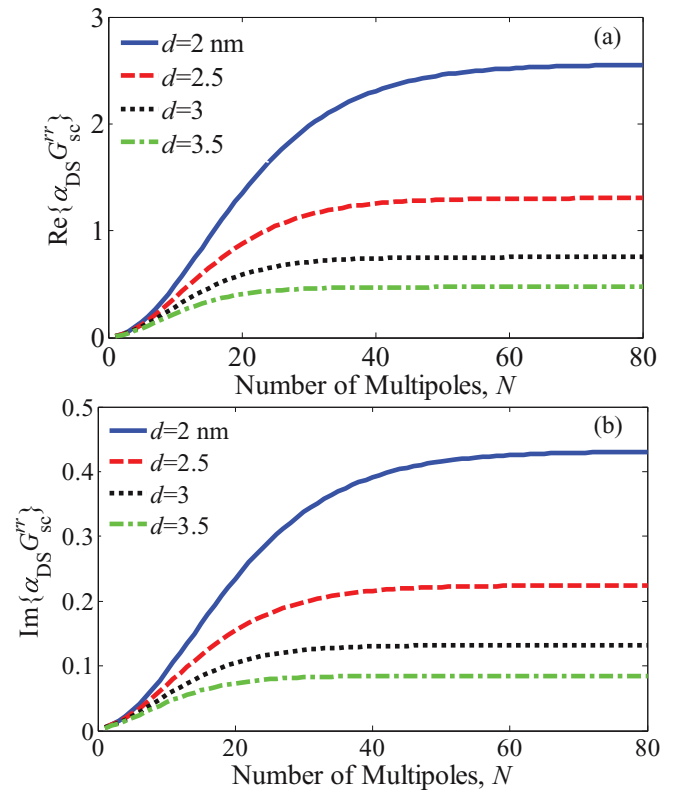


FIG. 9. (Color online) Convergence of G_{sc}^{rr} for $r_{PN} = 30$ nm and various values d of the distance between PN and the DS.

and

$$G_0^{rr}(\mathbf{r}, \mathbf{0}) = G'_0 + iG''_0. \quad (12)$$

For very subwavelength r_{PN} and d , PN-DS distance, $r = r_{PN} + d$ is subwavelength, and approximately one has G''_0/G'_0 of the order of $(kr)^3 \ll 1$, hence G''_0 is negligible and the approximation $G_0^{rr}(\mathbf{r}, \mathbf{0}) \approx G'_0$ holds. However, trends in the near field of G_{sc}^{rr}/G_{sc} are not straightforward because of the sum of several PN multipoles whose impact varies based on the physical parameters. To better illustrate these concepts, Figs. 10(a) and 10(b) show G''_0/G'_0 and G''_{sc}/G'_{sc} , respectively, versus DS distance d and PN radius r_{PN} . As expected G''_0/G'_0 is very small and can be easily neglected for the whole range of r_{PN} and d shown. However, G''_{sc}/G'_{sc} (using a gold PN) ranges between 0.16 and 0.24, and hence it is not much smaller than unity and it should be taken into account; in other words, both the real and imaginary parts of $G_{sc}^{rr}(\mathbf{r}, \mathbf{r})$ play a role in the excitation-rate enhancement. We want to stress that the behavior of G''_{sc}/G'_{sc} is highly dependent on the PN physical parameters and constituents, thus it needs to be analyzed on a case-to-case basis. Based on the real and imaginary parts introduced above, Eqs. (7) and (8) can be rewritten as

$$\bar{\gamma}_{exc}^n = |1 + \alpha'_{PN} G'_0 + i\alpha''_{PN} G''_0|^2 \quad (13)$$

$$\chi = \frac{1}{|1 + \alpha''_{DS} G''_{sc} - \alpha'_{DS} G'_{sc} - i(\alpha'_{DS} G''_{sc} + \alpha''_{DS} G'_{sc})|^2}. \quad (14)$$

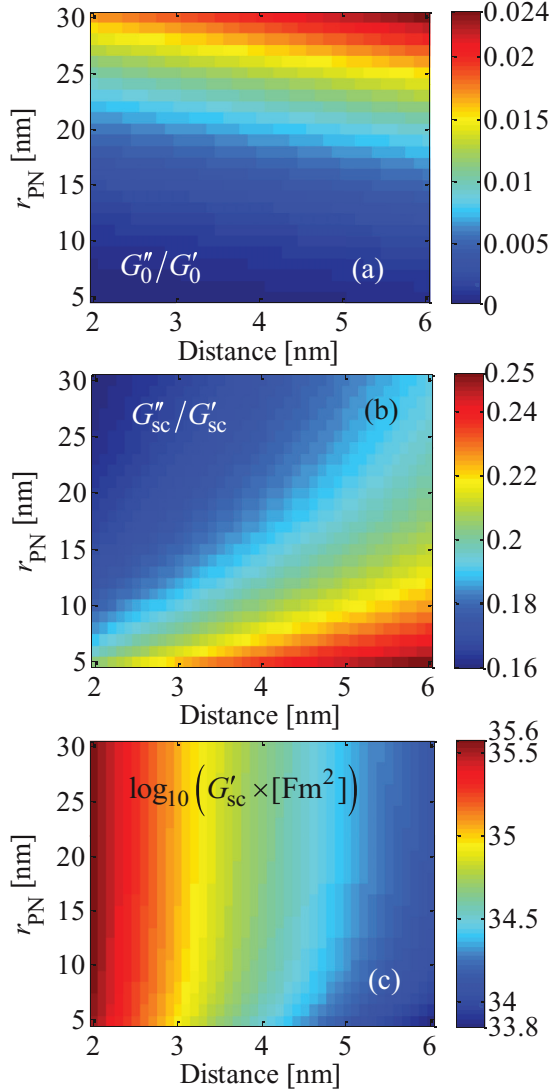


FIG. 10. (Color online) Plots of (a) G''_0/G'_0 , (b) G''_{sc}/G'_{sc} , and (c) G'_{sc} in logarithmic scale, versus the PN radius r_{PN} and d , at the frequency of 568 THz (528 nm).

Let us now investigate criteria for which we are able to achieve excitation-rate enhancement, associated to $\chi \gg 1$. Ideally, the strongest enhancement ($\chi \rightarrow \infty$) of the excitation rate is achieved when both

$$\begin{aligned} \text{Condition 1: } & A = 1 + \alpha''_{\text{DS}} G''_{\text{sc}} - \alpha'_{\text{DS}} G'_{\text{sc}} \approx 0 \\ \text{Condition 2: } & B = \alpha'_{\text{DS}} G''_{\text{sc}} + \alpha''_{\text{DS}} G'_{\text{sc}} \approx 0 \end{aligned} \quad (15)$$

are simultaneously satisfied. Using the above definitions, it is convenient to write

$$\chi = \frac{1}{A^2 + B^2}. \quad (16)$$

To maximize χ we need to minimize $A^2 + B^2$. Considering a gold PN, $G''_{\text{sc}} > 0$ and $G'_{\text{sc}} > 0$ as shown in Figs. 10(b) and 10(c). Also, we only consider the excitation regime of DSs, which implies $\alpha''_{\text{DS}} > 0$, i.e., passive, absorptive systems, though active dipolar scatterers can also be treated with

this theory. In general, α'_{DS} may assume both negative and positive values, especially when DSs exhibit a Lorentzian-like polarizability.

If we now consider the case with $\alpha'_{\text{DS}} < 0$, it follows that A is always positive and larger than 1 for gold PN. Therefore, $A^2 + B^2 > 1$ regardless of the value of B . That means χ is always less than 1 and self-coupling does not lead to enhancement. Therefore, $\alpha'_{\text{DS}} < 0$ is not a case of interest.

Instead, if we consider the case with $\alpha'_{\text{DS}} > 0$ (as in the structures analyzed in the previous sections), we note that both terms $\alpha'_{\text{DS}} G''_{\text{sc}}$ and $\alpha''_{\text{DS}} G'_{\text{sc}}$ in Condition 2 in Eq. (15) are positive in near field. It then follows that B is always positive, whereas A can vanish, which in turn would lead to $\chi = 1/B^2$. Therefore, a set of α'_{DS} and α''_{DS} here referred to as critical polarizabilities for a given distance d (or critical distances for a given polarizability α_{DS}), can lead to $\chi \gg 1$ by minimizing B and having $A = 0$, as discussed next.

Imposing Condition 1 (in the case of interest with $\alpha'_{\text{DS}} > 0$) is equivalent to

$$\alpha'_{\text{DS}} \approx \frac{1 + \alpha''_{\text{DS}} G''_{\text{sc}}}{G'_{\text{sc}}}, \quad (17)$$

which, when substituted in Condition 2, leads to

$$B \approx (1 + \alpha''_{\text{DS}} G''_{\text{sc}}) \frac{G''_{\text{sc}}}{G'_{\text{sc}}} + \alpha''_{\text{DS}} G'_{\text{sc}}. \quad (18)$$

We want to remark that in Eq. (18) three parameters (α''_{DS} , G'_{sc} , and G''_{sc}), which determine the value of α'_{DS} in Eq. (17), play an important role in the enhancement definition. Figures 10(b) and 10(c) show that G'_{sc} is of the order of $10^{35} [\text{F}^{-1}\text{m}^{-2}]$ and that $G''_{\text{sc}}/G'_{\text{sc}}$ is around 0.2. Also for the cases studied in previous sections, typical values of the imaginary part of the DS polarizability, α''_{DS} , are smaller than $10^{-36} [\text{F}^{-1}\text{m}^{-2}]$. Thus, in our cases, typically, $\alpha''_{\text{DS}} G''_{\text{sc}} < 0.02 \ll 1$; therefore, Eqs. (17) and (18) lead to

$$\alpha'_{\text{DS}} \approx \frac{1}{G'_{\text{sc}}} \quad \text{and} \quad B \approx \frac{G''_{\text{sc}}}{G'_{\text{sc}}} + \alpha''_{\text{DS}} G'_{\text{sc}} \ll 1. \quad (19)$$

In Eq. (19), the parameter B cannot be zero for the discussed setup (i.e., absorptive DS very close to a gold PN), and such an exact condition ($B = 0$) would require an emitting dye (i.e., $\alpha''_{\text{DS}} < 0$), not analyzed in this paper. Therefore, we interpret the value of $B \ll 1$ in Eq. (19) as a ‘‘penalty condition’’ rather than an optimum condition, which, however, still leads to (relatively) large enhancement factor χ . In the expression of B in Eq. (19), even if $\alpha''_{\text{DS}} G''_{\text{sc}} \ll G''_{\text{sc}}/G'_{\text{sc}}$, the value of $G''_{\text{sc}}/G'_{\text{sc}}$ is finite and nonzero, independent of DS polarizability, and imposed by only geometrical and material parameters. Therefore, the minimum value of B (and thus the maximum value of $\chi = 1/B^2$) for our specific setup is fixed and cannot be further optimized when using absorptive DSs. We recall from the setup pertaining to Fig. 3 that the polarizability $\alpha_{\text{DS}} \approx 9 \times 10^{-36} (1 + i0.01) [\text{Fm}^2]$ satisfies $\alpha'_{\text{DS}} \approx 1/G'_{\text{sc}}$ and $\alpha''_{\text{DS}} G''_{\text{sc}} \ll 1$. When using this value in Eq. (18) indeed one obtains small $B \approx G''_{\text{sc}}/G'_{\text{sc}} = 0.2$, through which we confirm a large enhancement of $\chi \approx 30$, as observed in Sec. III and shown in Fig. 3. Notice that the value of G'_{sc} [shown in Fig. 10(c)] is almost independent from the PN radius and the fact that $\alpha'_{\text{DS}} \approx 1/G'_{\text{sc}}$ explains why χ and the critical

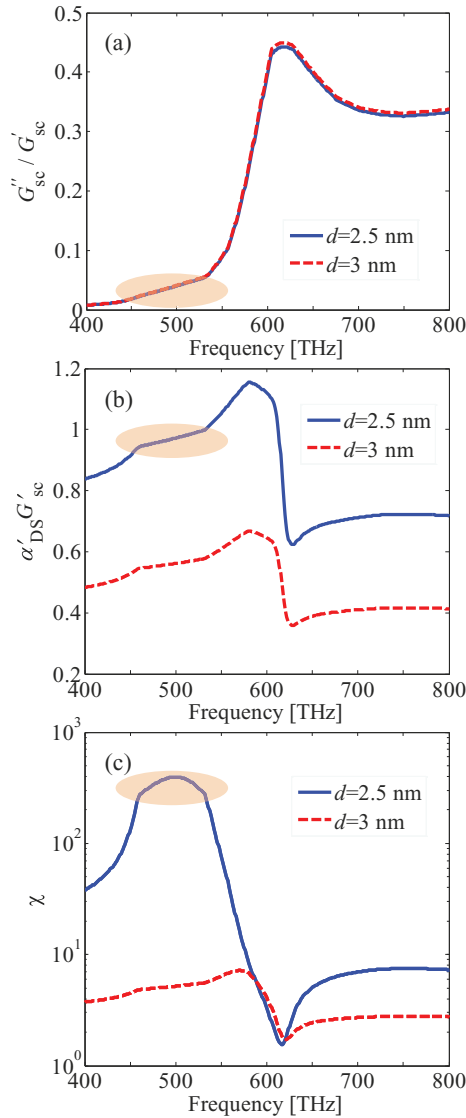


FIG. 11. (Color online) Plots of (a) G''_{sc}/G'_{sc} , (b) $\alpha'_{DS}G'_{sc}$, and (c) χ , the latter in logarithmic scale, versus frequency for two values of the distance d . The orange oval indicates the region where Eq. (19) is satisfied and leads to further enhancement.

polarizability exhibit the same independence (from PN radius) in Figs. 3(a) and 3(b), assuming constant d . On the other hand, when increasing the distance d in Fig. 4, the critical polarizability leading to strong enhancement also increases. This is justified by this analysis observing the decrease of G'_{sc} versus increasing d as shown in Fig. 10(c), as dictated by Eq. (19), which states $\alpha'_{DS} \approx 1/G'_{sc}$.

For the sake of providing the significance of critical distance, we now resort again to a DS Lorentzian polarizability as in Fig. 5. In Fig. 11 we show the variation of the parameters G''_{sc}/G'_{sc} , $\alpha'_{DS}G'_{sc}$, and χ versus frequency, for two values of the DS-PN distance d . One can see that for both values of d , $G''_{sc}/G'_{sc} \ll 1$ and $\alpha'_{DS}/\alpha_{DS} \ll 1$ in the frequency band 400–550 THz, as required to obtain large χ . However, while for $d = 3$ nm the value of $\alpha'_{DS}G'_{sc}$ is not close to unity, it is remarkable that for $d = 2.5$ nm $\alpha'_{DS}G'_{sc}$ is close to

unity in a certain frequency range (400–550 THz), leading to enhancements as large as 400 folds, shown in Fig. 11(c), remarking the importance of the concept of critical distance.

VI. CONCLUSION

Self-coupling has been neglected in almost all previous literature for the determination of the excitation rate and its enhancement. Here we have shown that this assumption leads to wrong estimates for certain critical physical parameters, off even by orders of magnitude in some special conditions. Indeed, we have shown that in some cases self-coupling is important and it is one of the major factors leading to large excitation-rate enhancements. The approach introduced here can be further extended to determine radiative and nonradiative decay rates as well as the emission-rate enhancement of a PN-DS system, and will be the subject of future investigation. The results shown in this paper may pave the way for the improvement of sensors based on local-field enhancement. Note that the concept of self-coupling as introduced here is very general and can be applied to nanostructures of any shape, used to enhance the local field. Strong enhancement due to self-coupling can be exploited only in very close proximity of the plasmonic nanoparticle.

ACKNOWLEDGMENTS

The authors acknowledge fruitful discussions with Prof. Eric Potma, Department of Chemistry, University of California, Irvine. Faezeh Tork Ladani acknowledges the support from the Broadcom Foundation.

APPENDIX: FREE SPACE AND SCATTERING DYADIC GREEN'S FUNCTIONS

The electric field at the observation \mathbf{r} from a dipolar scatterer located at \mathbf{r}' is expressed as

$$\mathbf{E}(\mathbf{r}) = \underline{\mathbf{G}}_i(\mathbf{r}, \mathbf{r}') \cdot \mathbf{p}, \quad (\text{A1})$$

where $i = \{“0”, “sc”\}$ refers to free space and scattering GF, respectively. The free space dyadic GF, $\underline{\mathbf{G}}_0(\mathbf{r}, \mathbf{r}')$ is given as

$$\underline{\mathbf{G}}_0(\mathbf{r}, \mathbf{r}') = \frac{e^{ikR}}{4\pi\epsilon_h\epsilon_0} \left[\left(\frac{k^2}{R} + \frac{ik}{R^2} - \frac{1}{R^3} \right) \mathbf{I} - \left(\frac{k^2}{R} + \frac{3ik}{R^2} - \frac{3}{R^3} \right) \hat{\mathbf{R}}\hat{\mathbf{R}} \right], \quad (\text{A2})$$

where $\mathbf{R} = R\hat{\mathbf{R}} = \mathbf{r} - \mathbf{r}'$ and \mathbf{I} is the identity dyad [6]. The scattering GF $\underline{\mathbf{G}}_{sc}(\mathbf{r}, \mathbf{r}')$ for a spherical scatterer at the origin of the coordinate system, is expressed based on the free space multipole expansion and Mie theory, which reads

$$\underline{\mathbf{G}}_{sc}(\mathbf{r}, \mathbf{r}') = \frac{-ik^3}{4\pi\epsilon_h\epsilon_0} \sum_{n=1}^{+\infty} \sum_{m=0}^n C_{mn} \times [A_n \mathbf{M}_{\sigma mn}^{(1)}(k\mathbf{r}) \mathbf{M}'_{\sigma mn}{}^{(1)}(k\mathbf{r}') + B_n \mathbf{N}_{\sigma mn}^{(1)}(k\mathbf{r}) \mathbf{N}'_{\sigma mn}{}^{(1)}(k\mathbf{r}')], \quad (\text{A3})$$

where A_n and B_n are the Mie coefficients for TE and TM modes, with respect to the radial direction, and \mathbf{M} and \mathbf{N}

are the corresponding spherical vector wave functions [35]. All the parameters in Eq. (A3) are defined in Ref. [35]. In particular,

$$A_n = \frac{j_n(\rho_2)[\rho_1 j_n(\rho_1)]' - j_n(\rho_1)[\rho_2 j_n(\rho_2)]'}{j_n(\rho_2)[\rho_1 h_n^{(1)}(\rho_1)]' - h_n^{(1)}(\rho_1)[\rho_2 j_n(\rho_2)]'}, \quad (\text{A4})$$

and

$$B_n = \frac{k_2^2 j_n(\rho_2)[\rho_1 j_n(\rho_1)]' - k_1^2 j_n(\rho_1)[\rho_2 j_n(\rho_2)]'}{k_2^2 j_n(\rho_2)[\rho_1 h_n^{(1)}(\rho_1)]' - k_1^2 h_n^{(1)}(\rho_1)[\rho_2 j_n(\rho_2)]'}, \quad (\text{A5})$$

where $j_n(\rho)$ and $h_n^{(1)}(\rho)$ are the spherical Bessel and Hankel functions, respectively [46], and a prime here refers to the first derivative with respect to the argument. Moreover, $\rho_2 = km_r r_{\text{PN}}$ and $\rho_1 = kr_{\text{PN}}$, with $m_r = \sqrt{\varepsilon_{\text{PN}}/\varepsilon_h}$ the relative refractive index contrast between the PN and the host medium, with ε_{PN} denoting the relative permittivity of the PN, and ε_h the one of the host medium. Here we assumed that the relative permeability is unitary. More general expressions of Eqs. (A4) and (A5) are in Ref. [5]. For calculation purposes, we limit the infinite n summation in Eq. (A3) to N multipolar terms that guarantee convergence, as discussed in Sec. IV.

-
- [1] C. Höppener and L. Novotny, *Q. Rev. Biophys.* **45**, 209 (2012).
 [2] R. H. Hadfield, *Nat. Photon.* **3**, 696 (2009).
 [3] E. Knill, R. Laflamme, and G. J. Milburn, *Nature* **409**, 46 (2001).
 [4] J. Wu, S. C. Mangham, V. R. Reddy, M. O. Manasreh, and B. D. Weaver, *Sol. Energy Mater. Sol. Cells* **102**, 44 (2012).
 [5] C. F. Bohren and D. R. Huffman, in *Absorption and Scattering of Light by Small Particles* (Wiley-VCH Verlag GmbH, Berlin, 1998).
 [6] F. Capolino and S. Steshenko, in *Theory and Phenomena of Metamaterials* (CRC Press, Boca Raton, 2009).
 [7] S. Campione, M. Albani, and F. Capolino, *Opt. Mater. Express* **1**, 1077 (2011).
 [8] S. Campione and F. Capolino, *Nanotechnology* **23**, 235703 (2012).
 [9] S. Xiao, V. P. Drachev, A. V. Kildishev, X. Ni, U. K. Chettiar, H.-K. Yuan, and V. M. Shalaev, *Nature* **466**, 735 (2010).
 [10] G. Strangi, A. De Luca, S. Ravaine, M. Ferrie, and R. Bartolino, *Appl. Phys. Lett.* **98**, 251912 (2011).
 [11] A. Ciattoni, R. Marinelli, C. Rizza, and E. Palange, *Appl. Phys. B* **110**, 23 (2013).
 [12] M. H. Chowdhury, J. R. Lakowicz, and K. Ray, *J. Phys. Chem. C Nanomater. Interfaces* **115**, 7298 (2011).
 [13] M. H. Chowdhury, S. K. Gray, J. Pond, C. D. Geddes, K. Aslan, and J. R. Lakowicz, *J. Opt. Soc. Am. B* **24**, 2259 (2007).
 [14] P. Anger, P. Bharadwaj, and L. Novotny, *Phys. Rev. Lett.* **96**, 113002 (2006).
 [15] R. Carminati, J.-J. Greffet, C. Henkel, and J. M. Vigoureux, *Opt. Commun.* **261**, 368 (2006).
 [16] Y. V. Vladimirova, V. V. Klimov, V. M. Pastukhov, and V. N. Zadkov, *Phys. Rev. A* **85**, 053408 (2012).
 [17] J. Gersten and A. Nitzan, *J. Chem. Phys.* **73**, 3023 (1980).
 [18] A. Moroz, *Opt. Commun.* **283**, 2277 (2010).
 [19] R. Ruppin, *J. Chem. Phys.* **76**, 1681 (1982).
 [20] M. Sukharev, N. Freifeld, and A. Nitzan, *J. Phys. Chem. C*, **118**, 10545 (2014).
 [21] G. Colas des Francs, A. Bouhelier, E. Finot, J. C. Weeber, A. Dereux, C. Girard, and E. Dujardin, *Optics Express* **16**, 17654 (2008).
 [22] K. Lopata and D. Neuhauser, *J. Chem. Phys.* **130**, 104707 (2009).
 [23] K. Lopata and D. Neuhauser, *J. Chem. Phys.* **131**, 014701 (2009).
 [24] D. Neuhauser and K. Lopata, *J. Chem. Phys.* **127**, 154715 (2007).
 [25] G. Khitrova, H. M. Gibbs, M. Kira, S. W. Koch, and A. Scherer, *Nat. Phys.* **2**, 81 (2006).
 [26] A. Salomon, C. Genet, and T. W. Ebbesen, *Angew. Chem.* **121**, 8904 (2009).
 [27] A. E. Schlather, N. Large, A. S. Urban, P. Nordlander, and N. J. Halas, *Nano Lett.* **13**, 3281 (2013).
 [28] J. Xie, Q. Fan, F. Xi, H. Xiao, Z. Tian, L. Zhang, J. Xu, Q. Ren, L. Zhou, P. K. Chu, and Z. An, *Plasmonics* **8**, 1309 (2013).
 [29] C. Conti, A. Di Falco, and G. Assanto, *Phys. Rev. E* **70**, 066614 (2004).
 [30] S. M. Adams, S. Campione, J. D. Caldwell, F. J. Bezares, J. C. Culbertson, F. Capolino, and R. Ragan, *Small* **8**, 2239 (2012).
 [31] X. Peng, L. Manna, W. Yang, J. Wickham, E. Scher, A. Kadavanich, and A. P. Alivisatos, *Nature* **404**, 59 (2000).
 [32] Hetch, *Philos. Trans. R. Soc. Math. Phys. Eng. Sci.* **362**, 881 (2004).
 [33] D. Ratchford, F. Shafiei, S. K. Gray, and X. Li, *ChemPhysChem* **13**, 2522 (2012).
 [34] S. Chandra, J. Doran, S. J. McCormack, M. Kennedy, and A. J. Chatten, *Sol. Energy Mater. Sol. Cells* **98**, 385 (2012).
 [35] C. Tai, *Dyadic Green Functions in Electromagnetic Theory* (IEEE Press, Piscataway, NJ, 1994).
 [36] A. Kinkhabwala, Z. Yu, S. Fan, Y. Avlasevich, K. Müllen, and W. E. Moerner, *Nat. Photon.* **3**, 654 (2009).
 [37] Z. Zhang, A. Weber-Bargioni, S. W. Wu, S. Dhuey, S. Cabrini, and P. J. Schuck, *Nano Lett.* **9**, 4505 (2009).
 [38] E. D. Palik, in *Handbook of Optical Constants of Solids*, edited by E. D. Palik (Academic Press, Burlington, 1997).
 [39] R. D. Artuso and G. W. Bryant, *Nano Lett.* **8**, 2106 (2008).
 [40] M. H. Chowdhury, S. Chakraborty, J. R. Lakowicz, and K. Ray, *J. Phys. Chem. C* **115**, 16879 (2011).
 [41] H. Xu and M. Käll, *Phys. Rev. Lett.* **89**, 246802 (2002).
 [42] E. C. Le Ru and P. G. Etchegoin, *Principles of Surface-Enhanced Raman Spectroscopy and Related Plasmonic Effects* (Elsevier, Boston/Amsterdam, 2009).
 [43] C. B. Murray, C. R. Kagan, and M. G. Bawendi, *Annu. Rev. Mater. Sci.* **30**, 545 (2000).
 [44] K. J. Webb and A. Ludwig, *Phys. Rev. B* **78**, 153303 (2008).
 [45] P. Holmström, L. Thylén, and A. Bratkovsky, *J. Appl. Phys.* **107**, 064307 (2010).
 [46] M. Abramowitz and I. A. Stegun, *Handbook of Mathematical Functions with Formulas, Graphs, and Mathematical Tables* (Dover Publications, New York, 1964).